






# Natural Coptidis Rhizoma Nanoparticles Improved the Oral Delivery of Docetaxel

Dan Ye <sup>1</sup>, Ding Ding<sup>1</sup>, Ling-Yun Pan<sup>2</sup>, Qing Zhao<sup>3</sup>, Long Chen <sup>2</sup>, Min Zheng <sup>1</sup>, Tong Zhang <sup>1</sup>, Bing-Liang Ma <sup>1</sup>

<sup>1</sup>Department of Pharmacology, School of Pharmacy, Shanghai University of Traditional Chinese Medicine, Shanghai, 201203, People's Republic of China; <sup>2</sup>Experiment Center for Science and Technology, Shanghai University of Traditional Chinese Medicine, Shanghai, 201203, People's Republic of China; <sup>3</sup>Department of Pharmacy, Jing'an District Zhabei Central Hospital, Shanghai, 200070, People's Republic of China

Correspondence: Bing-Liang Ma; Tong Zhang, Department of Pharmacology, School of Pharmacy, Shanghai University of Traditional Chinese Medicine, No. 1200 Cai Lun Road, Pudong New District, Shanghai, 201203, People's Republic of China, Tel +86-021-5132 2199; +86-021-5132 2318, Fax +86-021-5132 2192, Email bingliang.ma@hotmail.com; zhangtongshutcm@hotmail.com

**Purpose:** Docetaxel (DTX) is a valuable anti-tumor chemotherapy drug with limited oral bioavailability. This study aims to develop an effective oral delivery system for DTX using natural nanoparticles (Nnps) derived from Coptidis Rhizoma extract.

**Methods:** DTX-loaded self-assembled nanoparticles (Nnps-DTX) were created using an optimized heat-induction strategy. Nnps-DTX's shape, size, Zeta potential, and in vitro stability were all carefully examined. Additionally, the study investigated the encapsulation efficiency, loading capacity, crystal form, and intermolecular interactions of DTX in Nnps-DTX. Subsequently, the solubility, release, cellular uptake, metabolic stability, and preclinical pharmacokinetics of DTX in Nnps-DTX were systematically evaluated. Finally, the cytotoxicity of Nnps-DTX was assessed in three tumor cell lines.

**Results:** Nnps-DTX was spherical in shape,  $138.6 \pm 8.2$  nm in size, with a Zeta potential of  $-20.8 \pm 0.6$  mV, a DTX encapsulation efficiency of  $77.6 \pm 8.5\%$ , and a DTX loading capacity of  $6.8 \pm 1.9\%$ . Hydrogen bonds, hydrophobic interactions, and electrostatic interactions were involved in the formation of Nnps-DTX. DTX within Nnps-DTX was in an amorphous form, resulting in enhanced solubility (23.3 times) and release compared to free DTX. Following oral treatment, the mice in the Nnps-DTX group had DTX peak concentrations 8.8, 23.4, 44.6, and 5.7 times higher in their portal vein, systemic circulation, liver, and lungs than the mice in the DTX group. Experiments performed in Caco-2 cells demonstrated a significant increase in DTX uptake by Nnps-DTX compared to free DTX, which was significantly inhibited by indomethacin, an inhibitor of caveolae-mediated endocytosis. Furthermore, compared to DTX, DTX in Nnps-DTX demonstrated better metabolic stability in liver microsomes. Notably, Nnps-DTX significantly reduced the viability of MCF-7, HCT116, and HepG2 cells.

**Conclusion:** The novel self-assembled nanoparticles considerably enhanced the cellular absorption, solubility, release, metabolic stability, and pharmacokinetics of oral DTX and demonstrated strong cytotoxicity against tumor cell lines.

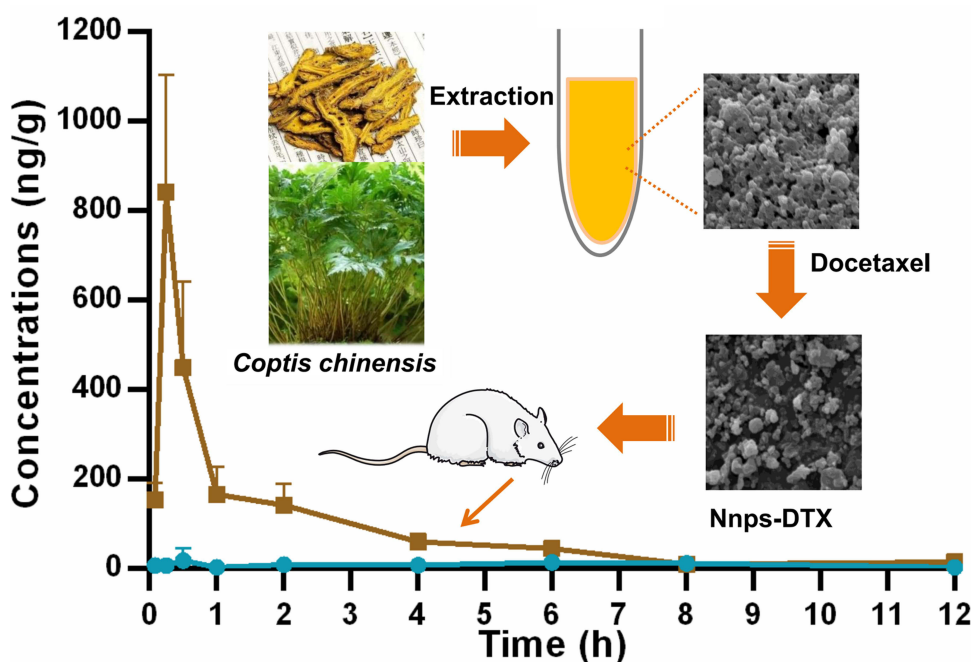
**Keywords:** docetaxel, oral delivery, self-assembly, nanoparticles, pharmacokinetics, coptidis rhizoma

## Introduction

Docetaxel (DTX), a semi-synthetic analog of paclitaxel, is one of the most valuable anti-tumor chemotherapy drugs.<sup>1</sup> DTX inhibits tumor cells by inducing tubulin polymerization into microtubules and inhibiting microtubule depolymerization.<sup>1</sup> Clinically, DTX is mainly used to treat locally advanced or metastatic breast cancer<sup>2</sup> and non-small-cell lung cancer.<sup>3</sup> Due to low water solubility, poor permeability, and extensive first-pass metabolism, the oral bioavailability of DTX is as low as 7.39%.<sup>4</sup> As a result, in clinical practice, DTX is administered via injection.<sup>1</sup> However, severe blood adverse events, primarily neutropenia,<sup>5</sup> are frequently brought on by injection-caused high blood concentrations. In addition, DTX injections cause allergic reactions.<sup>5</sup>

Oral DTX preparation with high bioavailability is one of the hottest areas of research.<sup>6</sup> Oral DTX has the advantage of being more effective and having fewer side effects than the injection, as oral DTX can be maintained in appropriate concentrations in the body for an extended duration.<sup>6</sup> For example, an oral nanoemulsion increased the oral bioavailability

## Graphical Abstract



of DTX by 2.49 times and had a stronger anti-breast cancer effect in experimental animals than conventional injections.<sup>4</sup> However, synthetic nanomaterials frequently include organic reagents, raising safety apprehensions.<sup>4,5</sup>

Drug carriers have the ability to attach drugs through both chemical bonding and physical adsorption, thereby regulating the rate of drug release and altering the manner and extent of drug entry into the body.<sup>7</sup> Natural proteins derived from animals and plants serve as effective carriers for drugs due to their excellent biodegradability and biocompatibility.<sup>8</sup> Human serum albumin (HSA), as an animal protein, is widely used for drug delivery due to its non-immunogenicity, good binding ability to most drugs, and certain tumor targeting.<sup>9</sup> For example, the HSA-paclitaxel complex does not require a co-solvent in the preparation process and can promote the uptake of paclitaxel by tumor cells, so it has good safety and efficacy.<sup>10</sup> Researchers have also explored constructing DTX nanoparticles using HSA.<sup>11,12</sup> However, because HSA is not readily available, animal derived albumin such as bovine serum albumin (BSA) is often used for drug delivery, including for DTX.<sup>13,14</sup> Nonetheless, the process of preparing nanoparticles based on animal proteins often requires the use of chemical linkers that are difficult to remove, and there are risks such as allergies and the transmission of animal diseases.<sup>8</sup> Nanoparticles made from plant proteins tend to exhibit better drug-release characteristics.<sup>8</sup> Consequently, novel carriers for DTX have emerged from plant proteins such as zein,<sup>15</sup> wheat germ agglutinin,<sup>16</sup> and soy protein isolate.<sup>17</sup> However, these plant proteins mentioned face challenges such as low solubility in water and instability.<sup>8</sup>

Coptidis Rhizoma refers to the dried rhizome of the medicinal plants including *Coptis chinensis* Franch, *C. dletoidea* C.Y. Cheng et Hasiao, or *C. teeta* Wall.<sup>18</sup> Previously, we isolated natural protein nanoparticles (Nnps) from the water extract of Coptidis Rhizoma.<sup>19</sup> The nanoparticles can significantly improve the pharmacokinetic properties of oral berberine hydrochloride,<sup>19,20</sup> the major bioactive constituent of Coptidis Rhizoma,<sup>18,21</sup> indicating the potential of these nanoparticles as effective carriers for oral drug delivery. Moreover, the water extract of Coptidis Rhizoma has a long history of oral use for treating various diseases in China.<sup>22</sup> Consequently, it is anticipated that the orally administered Nnps would demonstrate favorable biodegradability and biocompatibility. In this research, a novel type of self-assembled nanoparticles containing DTX (referred to as Nnps-DTX) was developed, and its suitability for the oral delivery of DTX was thoroughly examined.

## Materials and Methods

### Materials

Carbamazepine, amiloride, filters (0.22  $\mu\text{m}$ ), and dialysis bag (3500 Da) were provided by Shanghai Yuanye Biological Co., Ltd. (Shanghai, China). Docetaxel, cytochalasin D, chlorpromazine HCl, indomethacin, and CCK-8 kits were obtained from Dalian Meilen Biotechnology Co., Ltd. (Dalian, China). The bicinchoninic acid (BCA) protein test kits, Coomassie blue staining solution, protein marker, horseradish peroxidase (HRP), 30% acrylamide-bisacrylamide (29:1) water solution, 10% SDS-PAGE resolving gel master mix, SDS-PAGE sample loading buffer, ammonium persulfate substitute, and periodic acid-Schiff staining kits were purchased from Shanghai Biyuntian Biotechnology Co., Ltd. (Shanghai, China). Pepsin was the product of neoFroxx GmbH (Einhausen, Germany). Trypsin was obtained from Beijing Solarbio Science & Technology Co., Ltd. Liver microsomes were the product of Beijing Oriental Rada Biotech Co., Ltd. (Beijing, China). Ammonium formate, trypsin, formic acid, and the culture medium Dulbecco's modified Eagle's medium (DMEM) were the products of Thermo Fisher Scientific (Massachusetts, USA). Fetal bovine serum (FBS) and penicillin-streptomycin solution were the products of Biological Industries (BioInd) (Beit-Haemek, Israel). Zoletil<sup>®</sup>50, an injection of tiletamine hydrochloride and zolazepam hydrochloride, was purchased from Virbac Trading (Shanghai) Co., Ltd. (Shanghai, China). Dimethyl sulfoxide (DMSO) was produced by Merck (New Jersey, USA). Methanol and acetonitrile were purchased from Honeywell Trading (Shanghai) Co., Ltd. (Shanghai, China). The reference compounds used in this study were of purity exceeding 98%.

The dried herbal pieces (NO. 211211) of *Coptidis Rhizoma* originated from the Sichuan province in China and were supplied by Shanghai Kang Qiao Herbal Pieces Co., Ltd. (Shanghai, China).

### Extraction, Isolation, and Identification of Nnps

The dried herbal pieces of *Coptidis Rhizoma* were crushed to powder, soaked in 10 times the volume of water for 1 h, and extracted with warm (50°C) water for 12 h. Then, the water extract was filtered with gauze and vacuum-dried at 50°C. Next, the dried extract was dissolved in water and sonicated for 1 h. After centrifugation for 10 min at 3000 rpm, the obtained supernatant was filtered through 0.22- $\mu\text{m}$  filters. The resulting solution was dialyzed (3500 D) thoroughly against water and the residues in the dialysis bag were collected and freeze-dried to obtain Nnps.

The methods and results for Nnps identification are detailed in the "[Supplementary material 1](#)". To summarize, the protein and carbohydrate levels in Nnps were measured using BCA or phenol-sulfuric acid assays, respectively. Moreover, to confirm protein glycosylation in Nnps, periodic acid-Schiff staining was done post gel electrophoresis. The potential presence of *O*-glycosidic bonds was determined via  $\beta$ -elimination reaction and ultraviolet spectrum analysis. Additionally, the protein's peptide profile within Nnps was analyzed using liquid chromatography-mass spectrometry following trypsin digestion.

### Quantitative Analysis of DTX

The samples were precipitated with three volumes of acetonitrile and centrifuged for 10 min at 16,000 rpm. Then, an equal volume of water was added to the resulting supernatant and thoroughly mixed. Next, the qualitative analysis of DTX was performed using a Waters ACQUITY ultra-performance liquid chromatography (UPLC) system (MA, United States) and an API 5500 mass spectrometer (Boston, MA, United States), which was equipped with an electrospray ionization source.

An ACQUITY BEH C<sub>18</sub> column (2.1  $\times$  100 mm, 1.7  $\mu\text{m}$ , Waters, MA, USA) was used for the separation with a mobile phase consisting of solvent A (1 mM ammonium formate aqueous solution) and solvent B (methanol) at 40°C. The optimized gradient elution was as follows: 0 min, 60% B; 1 min, 60% B; 3.5 min, 90% B; 4.0 min, 60% B; 5.5 min, 60% B. The flow rate was 0.3 mL/min, and the injection volume was 10  $\mu\text{L}$ . In positive ion modes, multiple reaction monitoring was adopted for the quantification of the following compounds:  $m/z$  808.4 $\rightarrow$ 527.4 for DTX,  $m/z$  237.0 $\rightarrow$ 193.4 for carbamazepine (used as internal standard, IS). The optimized ion spray and the entrance potential were set at 5.5 kV and  $\pm$  10 V, respectively. The source temperature was maintained at 280°C. Nitrogen was used as the curtain gas (40 psi), auxiliary gas (50 psi), and nebulizer gas (50 psi). By using Analyst software (version 1.5.2, Applied

Biosystems), data were acquired and analyzed. The established liquid chromatography-tandem mass spectrometry (LC-MS/MS) method demonstrated good linearity over a concentration range of 0.39–800.0 ng/mL and met the requirements of quantitative analysis of DTX.

## Dynamic Light Scattering Analysis

The water solution containing Nnps-DTX at a concentration of approximately 1 mg/mL was prepared. After thoroughly vortex, the particle size, polydispersity index (PDI), and Zeta potential of the nanoparticles were subsequently assessed using a Malvern Zetasizer Nano analyzer (Worcestershire, UK).

## Optimization of Preparation Strategy of Nnps-DTX

### pH-Induced Self-Assembly Strategy

The lyophilized powder of Nnps was reconstituted in water and shaken for 2 hours. The resulting solution was left at 4°C overnight. After centrifugation at 10,000 rpm for 10 minutes and removal of undissolved Nnps, the Nnps concentration was adjusted to 1 mg/mL based on BCA analysis. Subsequently, the solution's pH was set to 2 or 12 with HCl or NaOH solutions, respectively, followed by stirring at 200 rpm for 0.5 hours. The ethanol solution of DTX was then gradually added to the Nnps solution, maintaining a final ethanol concentration below 1% and a DTX to Nnps ratio of 0.4. Throughout this process, continuous stirring was maintained. After an additional 2 hours of stirring, the solution's pH was readjusted to 7.0 with NaOH or HCl solution. The solution was then stirred overnight. Undissolved DTX or over-aggregated Nnps in the solution were removed by centrifugation at 10,000 rpm for 10 minutes. The size, Zeta potential, and PDI of the DTX-loaded nanoparticles (Nnps-DTX) in the supernatant were determined through DLS analysis.

### Alcohol-Induced Self-Assembly Strategy

The primary procedures mirrored those outlined in the section “pH-induced self-assembly strategy”, with two distinctions: (1) the pH was sustained at 7.0, and (2) the ultimate ethanol concentration varied at 1%, 20%, or 40%, respectively.

### Heat-Induced Self-Assembly Strategy

The primary procedures were identical to those explained in the section “pH-induced self-assembly strategy”. However, two variations were present: (1) The freeze-dried powder of Nnps was dissolved in water and subsequently heated at 65°C, 70°C, or 75°C for 0.5 hours; (2) the pH level was consistently kept at 7.0.

## Optimization of the Heat-Induced Self-Assembly Strategy

### Influencing Factors

The influence of Nnps concentration, DTX-Nnps ratios, environmental pH, and heating temperature on Nnps-DTX preparation were investigated. (1) The influence of Nnps concentration (0.6, 0.8, and 1 mg/mL) on Nnps-DTX were investigated under the conditions of a heating temperature of 65°C, a DTX-Nnps ratio of 0.4, and a pH value of 10. (2) The influence of DTX-Nnps ratios (0.2, 0.3, and 0.4) on Nnps-DTX were investigated at 65°C, 1 mg/mL protein, and a pH value of 10. (3) The influence of environmental pH (8, 9, and 10) on Nnps-DTX were investigated at a heating temperature of 65°C, a protein concentration of 1 mg/mL, and a DTX-Nnps ratio of 0.4. (4) The effects of heating temperature (65°C, 70°C, or 75°C) were tested in the section “Heat-induced self-assembly strategy”. The size, Zeta potential, and PDI of the prepared Nnps-DTX were determined by DLS analysis.

### Orthogonal Experiments

Based on the findings from section “Influencing factors”, a series of orthogonal designed experiments with four factors and three levels were conducted and replicated thrice.

### Optimized Procedure and Validation Experiment

Nnps-DTX was prepared according to the optimized procedure determined by the orthogonal experiments. Briefly, the aqueous solution of Nnps (2 mg/mL) was heated to 65°C and the undissolved fraction was removed by centrifugation at 10,000 rpm for 10 min. The protein content of the supernatant was determined and adjusted to 1 mg/mL based on BCA

analysis. An ethanol solution (final concentration less than 1%) of DTX (final concentration 0.3 mg/mL) was added with stirring. The pH of the solution was adjusted to 10 and stirring continued overnight. After centrifugation at 10,000 rpm for 10 min, the size, Zeta potential, and PDI of the nanoparticles in the supernatant obtained were determined by DLS analysis. The supernatant was then lyophilized to obtain the powder of Nnps-DTX.

## Characterization of Nnps-DTX

### In vitro Stability of Nnps-DTX

The lyophilized powder of Nnps-DTX was accurately weighed and dissolved to a concentration of 1 mg/mL in water, artificial gastric fluid (water containing 2.0 g/L sodium chloride, pH adjusted to 1.2 with hydrochloric acid and sodium hydroxide),<sup>23</sup> or artificial intestinal fluid (water containing 0.2 mol/L sodium phosphate, pH adjusted to 6.8 with hydrochloric acid and sodium hydroxide).<sup>24</sup> Additionally, pepsin (0.32%, w/v)<sup>25</sup> and trypsin (1%, w/v)<sup>25</sup> were introduced to the artificial intestinal fluid and gastric fluid, respectively, to assess the impact of the digestive enzymes on the stability of Nnps-DTX. Undissolved Nnps-DTX powder was removed by centrifugation at 10,000 rpm for 10 minutes, and the supernatant was collected and left for a specified time (water: 0, 1, 2, 4, and 6 hours, respectively; artificial gastric fluid: 0, 30, 60, 90, and 120 minutes, respectively; artificial intestinal fluid: 0, 1, 2, 4, and 6 hours, respectively). At each time point, a certain volume of the supernatant was sampled, and the size, PDI, and Zeta potential of the nanoparticles in the supernatant were immediately measured.

### Encapsulation Efficiency (EE) and Drug Loading (DL) of DTX

The lyophilized powder of Nnps-DTX was precisely weighed and recorded as  $M_{\text{total}}$ . Next, water was added to prepare 4 mL of a fully dispersed nanoparticle solution at a concentration of 1 mg/mL.

After that, 2 mL of the suspension was placed in a volumetric bottle, and methanol was added to 10 mL and weighed. After the ultrasound for 30 min, methanol was added to make up the missing weight. The solution was centrifuged at 10,000 rpm for 10 min, and then the concentration of DTX in the obtained supernatant was detected. The total amount of DTX in the Nnps-DTX powder was calculated according to the concentration and volume, and recorded as  $M_{\text{total DTX}}$ .

Another 2 mL of the Nnps-DTX suspension was placed in ultrafiltration centrifuge tubes (with an interception molecular weight of 3 kDa). After centrifugation for 20 min at 9000 rpm, the filtrate was collected to detect the concentration of DTX. The total amount of free DTX in the Nnps-DTX powder was calculated according to the concentration and volume and recorded as  $M_{\text{free DTX}}$ .

The EE and DL values of DTX in Nnps-DTX were calculated according to the following formulas:

$$EE = (M_{\text{total DTX}} - M_{\text{free DTX}}) / M_{\text{total DTX}} \times 100\%$$

$$DL = (M_{\text{total DTX}} - M_{\text{free DTX}}) / (M_{\text{total}} - M_{\text{total DTX}}) \times 100\%$$

### Crystal Form of DTX in Nnps-DTX

The shapes of DTX, Nnps, and Nnps-DTX were observed by scanning electron microscopy (SEM). Briefly, after being sprayed with gold, dried in a vacuum, the powder of DTX, Nnps, or Nnps-DTX were observed using an FEI Quanta 250 SEM (Oregon, USA), which was operated at 10 kV. Furthermore, the crystal form of DTX in Nnps-DTX was analyzed with the methods of differential scanning calorimetry (DSC) and powder X-ray diffraction (PXRD). DSC analysis was performed using a TA DSC Q2000 differential scanning calorimeter (Delaware, USA). In brief, the sample powder (about 1.5 mg) was placed into an open aluminum crucible and then heated from 20°C to 320°C at a rate of 10°C/min. PXRD analysis was performed using a Bruker D2 phaser (Rheinstetten, Germany) system. The operating conditions were as follows: The voltage was 30.0 kV, the current was 10.0 mA, the scanning range was 3°–40°, the increment was 0.02°, and the scanning speed was 0.1 s per step.

## Fourier Transform Infrared Spectroscopy (FTIR) Analysis

Briefly, KBr (190 mg) was used to individually grind 10.0 mg of DTX, Nnps, or Nnps-DT powders into fine powders, which were then respectively compacted into pellets. Subsequently, a Thermo Scientific Nicolet™ iS20 FTIR

spectrometer (Waltham, MA, USA) was used to obtain the FTIR spectra of each sample at a resolution of  $4\text{ cm}^{-1}$  and in the range of  $4000\text{--}500\text{ cm}^{-1}$ .

## Water Solubility of DTX in Nnps-DTX

Supersaturated water solutions of DTX (1 mg/mL) and lyophilized powder of Nnps-DTX (containing 1 mg/mL DTX) were prepared, respectively. After 60 min of ultrasonic treatment, the solutions were centrifuged at 16,000 rpm for 10 min, and the supernatant was collected and then diluted with 50% methanol-water containing the internal standard carbamazepine. The concentration of DTX in the supernatant was determined using the LC-MS/MS method.

## Release of DTX in Artificial Gastric and Intestinal Fluids

The lyophilized powder of Nnps-DTX or DTX was weighed and added into the artificial gastric fluid or artificial intestinal fluid, which had a pH of 1.2 or 6.8, respectively. The final concentration of DTX in the buffers was 0.2 mg/mL. About 1 mL of the buffer was loaded into a dialysis bag with a molecular weight cutoff of 3500 Da. Next, the dialysis bag was placed in a beaker containing 100 mL of the dissolution medium, ie, the hydrochloric acid buffer or phosphate buffer. The beaker was then placed in a water bath at  $37^\circ\text{C}$  with low-speed stirring (50 rpm). For the dissolution experiment in the buffer of hydrochloric acid, samples were obtained at 5, 15, 30, 45, 60, 90, and 120 min, respectively. For the dissolution experiment in phosphate buffer, samples were obtained at 5, 15, and 30 min, 1, 1.5, 2, 3, 4, 6, and 8 h, respectively. The sample volume was 800  $\mu\text{L}$ , and the same volume of blank buffer was replenished after sampling. The concentration of DTX was measured by the LC-MS/MS method.

## Metabolism of DTX in Liver Microsomes

DTX and Nnps-DTX, both containing a  $10\text{-}\mu\text{M}$  final concentration of DTX, were mixed with mouse liver microsomes (0.5 mg/mL) in a  $100\text{-}\mu\text{L}$  phosphate buffer solution (100 mM, pH 7.4) and then pre-incubated for 5 min at  $37^\circ\text{C}$ . Then, reduced nicotinamide adenine dinucleotide phosphate (NADPH, with a final concentration of 1 mg/mL) was added to initiate the *in vitro* metabolism of DTX. The metabolism of DTX was terminated after incubation for 0.5 or 1.5 h with the same volume of chilled (about  $4^\circ\text{C}$ ) acetonitrile, which contained carbamazepine that was used as the internal standard. After centrifugation for 5 min at 14,000 rpm, the supernatant was collected. The concentration of DTX was detected using the LC-MS/MS method. The metabolic stability of DTX was assessed by measuring the percentage of metabolized DTX.

## Uptake of DTX in Caco-2 Cells

Human colonic adenocarcinoma cells (Caco-2) were obtained from the National Collection of Authenticated Cell Cultures (Shanghai, China). The cells were cultured in DMEM containing 10% FBS, penicillin-streptomycin solution, and HEPES (15 mM) at  $37^\circ\text{C}$  in a humidified atmosphere of 5%  $\text{CO}_2$ . Hank's balanced salt solution [HBSS, 135 mM NaCl, 1.2 mM  $\text{MgCl}_2$ , 0.81 mM  $\text{MgSO}_4$ , 27.8 mM glucose, 2.5 mM  $\text{CaCl}_2$ , and 25 mM HEPES, pH 7.2] was used instead of the DMEM medium in drug-treating experiments. When DMSO was used, its final concentration was restricted to less than 1%.

Caco-2 cells were cultured in 12-well plates until the confluence reached 80–90%. The medium was replaced with a new medium 2 h before the experiment. Then the cells were washed with HBSS and divided into 6 groups, ie, DTX, Nnps-DTX, and Nnps-DTX plus one of the endocytosis inhibitors (the inhibitor of caveolae-mediated endocytosis, indomethacin, 100  $\mu\text{g/mL}$ ;<sup>26</sup> the inhibitor of clathrin-mediated endocytosis, chlorpromazine, 10  $\mu\text{g/mL}$ ;<sup>26</sup> the macropinocytosis inhibitor, amiloride, 2.5 mM;<sup>27</sup> and the phagocytosis, inhibitor cytochalasin D, 5  $\mu\text{M}$ <sup>27</sup>). The cells were incubated with blank HBSS (only for DTX and Nnps-DTX) or the inhibitors for 1 h. Next, the cells were incubated with DTX (10  $\mu\text{M}$ , only for the DTX group) or Nnps-DTX (containing 10  $\mu\text{M}$  DTX for the rest of the groups) for 4 h. The cells were then washed three times with chilled HBSS after the culturing medium was removed. The cells were digested with trypsin and centrifuged at 1000 rpm for 2 min to collect the cells. After washing twice with cold HBSS, the cells were suspended in chilled water and broken by the repeated freeze-thaw method. The DTX concentration was determined

by the LC-MS/MS method, the protein concentration of each sample was determined by the BCA kits, and then the DTX concentration in each sample was normalized by protein content.

## Pharmacokinetics of DTX in Mice

Male Kunming mice (specific pathogen-free grade, 22–24 g) were purchased from Beijing Vital River Laboratory Animal Technology Co. Ltd. (Beijing, China), which holds the production license of SCXK (Beijing) 2021–0006. The mice were maintained in air-conditioned rooms with a temperature of 22–24°C and a 12-hour light/dark cycle. Mice were fasted overnight before the experiment but were allowed to drink water *ad libitum*. All animal experiments were approved by the Institutional Animal Care and Use Committee of Shanghai University of Traditional Chinese Medicine (SHUTCM) under the approval number PZSHUTCM211018015. In addition, animal experiments were performed according to the guidelines of the committee at the laboratory animal center of SHUTCM, which holds the experimental license of SYXK (Shanghai) 2020–0009.

Ninety male KM mice were used in this experiment. According to body weight, the mice were randomly divided into two large groups, each of which contained nine small groups. Therefore, there were five mice in each small group. In order to obtain the water solutions of DTX, the powders were successively dispersed in pure water, vortexed, and sonicated for half an hour. As for Nnps-DTX, the powders were dispersed in pure water and vortexed. The mice were orally administered a water solution of DTX (20 mg/kg) or Nnps-DTX containing the same dose of DTX, respectively. At each time point (0.125, 0.25, 0.5, 1, 2, 4, 6, 8 or 12 h) after administration, five mice were anaesthetized with Zoletil® 50 and the portal vein and systemic blood were collected to prepare plasma with heparin anticoagulation. The liver and lungs were subsequently excised, rinsed with frozen saline solution, and quantified in terms of weight. The anaesthetized mice were then euthanized by cervical dislocation. Tissue homogenates were prepared using chilled water. Plasma and tissue homogenates were frozen at –80°C. After protein precipitation with three times the volume of acetonitrile, the DTX concentrations in the biological samples were determined by LC-MS/MS.

## In vitro Cytotoxicity of Nnps-DTX

Three cell lines, including MCF-7 (a human breast cancer cell line), HepG2 (a human liver carcinoma cell line) and HCT116 (a human colon tumor cell line), were obtained from the National Collection of Authenticated Cell Cultures (Shanghai, China). Cells were cultured at 37°C in a humidified atmosphere of 5% CO<sub>2</sub> in DMEM medium. The medium was supplemented with 10% heat-deactivated FBS, penicillin (100 U/mL), streptomycin sulphate (100 mg/mL), sodium pyruvate (1 mM) and HEPES (15 mM).

The weighed pure DTX, Nnps and NPS-DTX were placed in sterile test tubes and sterilized overnight at –80°C in a refrigerator. DTX was then dissolved in DMSO at a concentration of 20 mg/mL and then diluted with culture medium to 0.3, 1, 3, 10, 30, 100 and 300 ng/mL, respectively. Nnps and NPS-DTX were dispersed directly into the culture medium. The concentrations of DTX in the NPS-DTX solution were equivalent to 0.3, 1, 3, 10, 30, 100 and 300 ng/mL, respectively. The concentrations of Nnps were equivalent to those in the Nnps-DTX group. Note that the final concentrations of FBS and DMSO in each solution were 2.5% and 0.5%, respectively.

Cells were seeded in 96-well plates and incubated with the prepared solutions of DTX, Nnps or NPS-DTX for 48 h. Then 10 µL of CCK-8 enhanced solution was added to each well and incubated for a further 1 h. The absorbance of each well at 490 nm was measured using the Multiskan SkyHigh microplate spectrophotometer. The percentage inhibition of cell viability was calculated by comparing the absorbance of each well with that of the control groups, and the IC<sub>50</sub> values were calculated.

## Data Analysis

Non-compartmental analysis was performed using WinNonlin® software (Pharsight, CA, USA) to obtain the pharmacokinetic parameters of DTX. Quantitative data were expressed as mean ± SD, and the statistical difference between means was compared by analysis of variance followed by Dunnett's test with the minimum level of significance ( $p < 0.05$ ).

## Results

### Optimization of Nnps-DTX Preparation Strategies

In general, when the pH and ethanol-induced self-assembly strategies were used, the prepared nanoparticles were large in size and poor in Zeta potential (Table 1). However, when the heat-induced self-assembly strategy was used, the size of the nanoparticles obtained was less than 200 nm and the Zeta potential was lower than  $-20$  mV (Table 1). Therefore, the heat-induced self-assembly strategy was adopted in subsequent studies.

### Optimization of the Heat-Induction Strategy

#### Influencing Factors

In addition to the temperature (Table 1), Table 2 demonstrates how the concentration of Nnps, DTX/Nnps ratio, and pH value of the incubation solution impacted the properties of Nnps-DTX.

When the Nnps concentration rose from 0.3 mg/mL to 1 mg/mL, the particle size of the nanoparticles decreased gradually but then increased when the concentration increased to 3 mg/mL. Moreover, the absolute value of the Zeta potential decreased as the Nnps concentration grew. The concentration of Nnps demonstrated a minimal impact on PDI. As the DTX/Nnps ratio rose from 0.05 to 0.2, the size and absolute Zeta potential of the nanoparticles gradually decreased. Nevertheless, upon exceeding a ratio of 0.3, both particle size and potential values increased. The impact of DTX/Nnps ratios on PDI was negligible. When the pH of the incubation solution was raised from 8 to 10, there was a decrease in both particle size and PDI, while the absolute value of the Zeta potential increased.

**Table 1** Nanoparticles Prepared via Self-Assembly Strategies (Mean  $\pm$  SD, n = 3)

Strategies	Values	Size (nm)	Zeta Potential (mV)	Polydispersity Index
pH Induction	2	657.3 $\pm$ 221.6	$-11.7 \pm 0.3$	0.65 $\pm$ 0.12
	12	286.5 $\pm$ 48.5	$-18.1 \pm 0.6$	0.41 $\pm$ 0.02
Ethanol Induction	1%	977.2 $\pm$ 387.2	$-15.1 \pm 1.4$	0.83 $\pm$ 0.12
	20%	545.5 $\pm$ 138.9	$-10.1 \pm 1.4$	0.38 $\pm$ 0.21
	40%	1010.3 $\pm$ 103.6	$-9.3 \pm 1.7$	0.19 $\pm$ 0.01
Heat Induction	65°C	183.5 $\pm$ 25.3	$-20.5 \pm 2.4$	0.36 $\pm$ 0.06
	70°C	176.2 $\pm$ 23.6	$-20.0 \pm 2.8$	0.40 $\pm$ 0.04
	75°C	194.1 $\pm$ 11.6	$-20.7 \pm 1.7$	0.52 $\pm$ 0.03

**Table 2** Factors Influencing Nanoparticle Properties (Mean  $\pm$  SD, n = 3)

Factors	Values	Size (nm)	Zeta Potential (mV)	Polydispersity Index
Nnps Concentration (mg/mL)	0.3	246.2 $\pm$ 48.3	$-32.3 \pm 6.6$	0.32 $\pm$ 0.06
	0.6	206.9 $\pm$ 42.0	$-29.4 \pm 3.4$	0.36 $\pm$ 0.05
	0.8	196.6 $\pm$ 21.2	$-28.5 \pm 2.5$	0.35 $\pm$ 0.04
	1	160.8 $\pm$ 21.4	$-24.4 \pm 3.1$	0.36 $\pm$ 0.06
	3	198.9 $\pm$ 34.4	$-11.8 \pm 0.7$	0.32 $\pm$ 0.07
DTX/Nnps ratio	0.05	189.4 $\pm$ 11.1	$-21.8 \pm 2.2$	0.26 $\pm$ 0.02
	0.1	182.8 $\pm$ 8.8	$-23.5 \pm 1.0$	0.32 $\pm$ 0.06
	0.15	178.9 $\pm$ 4.5	$-21.4 \pm 0.6$	0.23 $\pm$ 0.01
	0.2	143.8 $\pm$ 0.8	$-17.6 \pm 2.6$	0.26 $\pm$ 0.05
	0.3	158.9 $\pm$ 2.1	$-18.8 \pm 1.5$	0.24 $\pm$ 0.01
pH value	8	189.0 $\pm$ 2.4	$-19.2 \pm 0.8$	0.33 $\pm$ 0.05
	9	178.4 $\pm$ 6.8	$-19.0 \pm 2.3$	0.30 $\pm$ 0.06
	10	168.1 $\pm$ 20.1	$-20.2 \pm 1.1$	0.27 $\pm$ 0.08



## Optimized Preparation Condition of Nnps-DTX

The outcomes of the orthogonal experiments can be found in Table 3. The variance analysis showed that the most important factor affecting particle size was the DTX/Nnps ratio ( $p < 0.01$ ), followed by pH value ( $p < 0.05$ ), and the optimal condition for particle size was A<sub>1</sub>B<sub>3</sub>C<sub>1</sub>D<sub>3</sub>. In addition, Nnps concentration ( $p < 0.05$ ) and pH value ( $p < 0.05$ ) had significant effects on Zeta potential, and the optimal condition for Zeta potential was A<sub>2</sub>B<sub>1</sub>C<sub>2</sub>D<sub>3</sub>. Furthermore, temperature had a significant effect on PDI ( $p < 0.05$ ), and the optimal condition for PDI was A<sub>1</sub>B<sub>1</sub>C<sub>1</sub>D<sub>3</sub>.

Finally, A<sub>1</sub>B<sub>3</sub>C<sub>2</sub>D<sub>3</sub> was determined as the optimal conditions for Nnps-DTX preparation, that is, the heating temperature was 65°C, the protein concentration was 1 mg/mL, the DTX/Nnps ratio was 0.3, and the pH value was 10.

## Validation Experiment

Nnps-DTX was prepared according to optimized conditions. The DLS analysis showed that the size of the nanoparticles was  $137.3 \pm 1.8$  nm, the Zeta potential was  $-19.4 \pm 1.7$  mV, and the PDI was  $0.46 \pm 0.00$ . Subsequently, the nanoparticle solution was lyophilized to obtain a powder form of Nnps-DTX. Finally, the powder was reconstituted in water at a concentration of 1 mg/mL. The DLS analysis revealed that the particles in the solution had a size of  $138.6 \pm 8.2$  nm with a PDI of  $0.24 \pm 0.02$ , and a Zeta potential of  $-20.8 \pm 0.6$  mV (Figure 1A). The findings suggested that lyophilization did not have a notable impact on the size and Zeta potential of Nnps-DTX nanoparticles.

## Characterization of Nnps-DTX

### In vitro Stability of Nnps-DTX

As shown in Figure 1B, the size and PDI of Nnps-DTX did not change significantly within 6 h in water and 2 h in artificial gastric fluid lacking pepsin, indicating its good stability in these solutions. In artificial intestinal fluid lacking trypsin, both size and PDI increased slightly compared to the control group measured immediately after preparation. The results suggested that the structure of the nanoparticles may have changed in the artificial intestinal fluid.

Notably, the digestive enzymes exerted significant effects on the size and PDI of Nnps-DTX. Following incubation in artificial gastric fluid containing pepsin, Nnps-DTX's size increased by more than 2 times (Figure 1B ii). Nnps-DTX's size was stable but PDI was increased after incubation in artificial intestinal fluid containing trypsin (Figure 1B iii). These findings suggest that the nanostructure of Nnps-DTX may undergo some degree of variation in the gastrointestinal tract following oral administration, likely due to the influence of digestive enzymes.

### EE and DL of DTX in Nnps-DTX

The EE and DL of DTX in Nnps-DTX were affected by treatments before freeze-drying. According to the results in Table 4, it was decided to obtain the freeze-dried Nnps-DTX powder after centrifugation at 10,000 rpm for 10 min. In addition, the content of DTX in Nnps-DTX freeze-dried powder was  $7.97 \pm 1.04\%$ .

**Table 3** Results of the Orthogonal Experiments (Mean  $\pm$  SD, n = 3)

Experiments	Factors				Responses		
	A	B	C	D	Size (nm)	Zeta Potential (mV)	Polydispersity Index
1	1	1	1	1	185.2 $\pm$ 5.9	-18.5 $\pm$ 3.2	0.26 $\pm$ 0.00
2	1	2	2	2	181.6 $\pm$ 28.4	-20.5 $\pm$ 1.6	0.31 $\pm$ 0.11
3	1	3	3	3	176.5 $\pm$ 26.8	-19.6 $\pm$ 2.1	0.33 $\pm$ 0.13
4	2	1	2	3	186.5 $\pm$ 24.6	-27.2 $\pm$ 2.9	0.33 $\pm$ 0.07
5	2	2	3	1	429.5 $\pm$ 186.8	-20.3 $\pm$ 0.9	0.53 $\pm$ 0.11
6	2	3	1	2	165.8 $\pm$ 6.4	-19.3 $\pm$ 1.9	0.33 $\pm$ 0.09
7	3	1	3	2	299.4 $\pm$ 81.8	-22.3 $\pm$ 1.5	0.46 $\pm$ 0.13
8	3	2	1	3	186.6 $\pm$ 22.9	-21.2 $\pm$ 2.0	0.36 $\pm$ 0.07
9	3	3	2	1	244.9 $\pm$ 60.6	-17.9 $\pm$ 0.9	0.57 $\pm$ 0.17

**Notes:** A, temperature (°C; 1, 2, 3: 65, 70, 75, respectively); B, Nnps concentration (mg/mL; 1, 2, 3: 0.6, 0.8, 1, respectively); C, docetaxel/Nnps ratio (1, 2, 3: 0.2, 0.3, 0.4, respectively); D, pH value (1, 2, 3: 8, 9, 10, respectively).

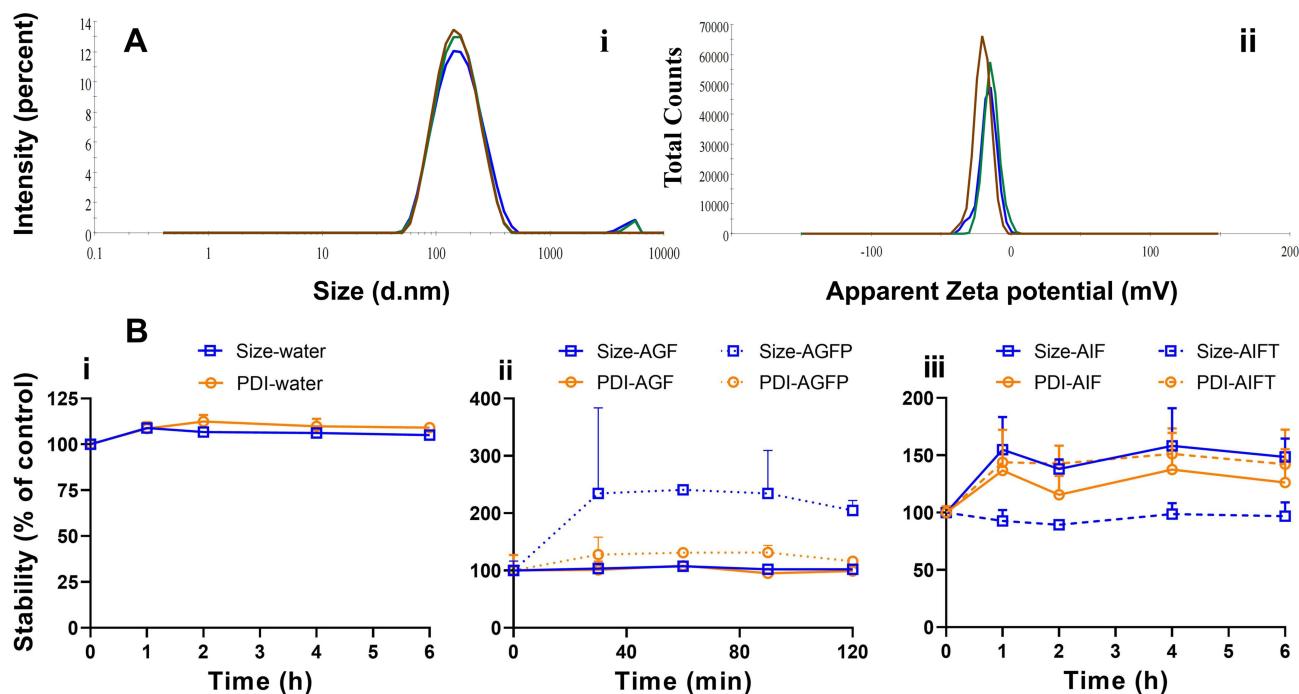


**Figure 1** Basic properties of the self-assembled nanoparticles loaded with docetaxel (Nnps-DTX). **(A)** particle size (i) and Zeta potential (ii) of the nanoparticles in the water solution of lyophilized Nnps-DTX powder. **(B)** size and polydispersity index (PDI) of Nnps-DTX after incubation in water (i), artificial gastric fluid with (AGFP) or without pepsin (AGF) (ii), and artificial intestinal fluid with (AIFT) or without trypsin (AIF) (iii), respectively (mean  $\pm$  SD,  $n = 3$ ). The groups at time point "0" were the control groups.

### Crystal Form of DTX in Nnps-DTX

SEM observations showed that DTX was in the form of long columnar crystals (Figure 2A), Nnps was spherical (Figure 2B), and Nnps-DTX (Figure 2C) was spherical without a columnar crystal structure. DSC analysis showed that the melting point of DTX was 169.63°C (Figure 2D), but the melting point of Nnps-DTX (Figure 2E) was not detected. The PXRD results showed that DTX (Figure 2G) had several strong diffraction peaks, but the diffraction peaks in Nnps-DTX (Figure 2I) disappeared. In addition, the Nnps themselves have no obvious melting point (Figure 2F) and diffraction peak (Figure 2H). These results suggest that DTX may exist in an amorphous state in the nanoparticles.

### FTIR Analysis

The FTIR spectra of DTX, Nnps, and NNPS-DTX are shown in Figure 3. The FTIR spectrum of DTX exhibited peaks at 3380, 2980, and 1714  $\text{cm}^{-1}$ , consistent with literature reports.<sup>28,29</sup> Nnps displayed characteristic peaks at 3304, 2933, and 1649  $\text{cm}^{-1}$ . The presence of a peak at 1649  $\text{cm}^{-1}$  indicated that the secondary structure of Nnps primarily comprises  $\alpha$ -helix and random coil structures.<sup>30</sup> In the spectrum of Nnps-DTX, the peak at 3388  $\text{cm}^{-1}$  (reflecting O-H and N-H stretching) was sharper and significantly shifted compared to those in Nnps (3304  $\text{cm}^{-1}$ ) and DTX (3380  $\text{cm}^{-1}$ ). Additionally, the characteristic peak at 1714  $\text{cm}^{-1}$  reflecting C=O stretching in DTX disappeared in the spectrum of Nnps-DTX. These findings suggest significant hydrogen bonding interactions between the C=O and OH groups of DTX with Nnps.<sup>31</sup> In the FTIR spectrum of Nnps-DTX, the peak at 2939  $\text{cm}^{-1}$  (reflecting C-H stretching) was shifted

**Table 4** Encapsulation Efficiency (EE) and Drug Loading (DL) of Docetaxel in the Nanoparticles (Mean  $\pm$  SD,  $n = 3$ )

Treatments Before Freeze-Drying	EE (%)	DL (%)
Centrifugation (10000 rpm, 10 min)	77.6 $\pm$ 8.5	6.8 $\pm$ 1.9
Centrifugation (3000 rpm, 10 min)	90.1 $\pm$ 1.3	5.5 $\pm$ 0.7
Filtration (0.22 $\mu\text{m}$ )	86.2 $\pm$ 2.7	3.7 $\pm$ 1.0

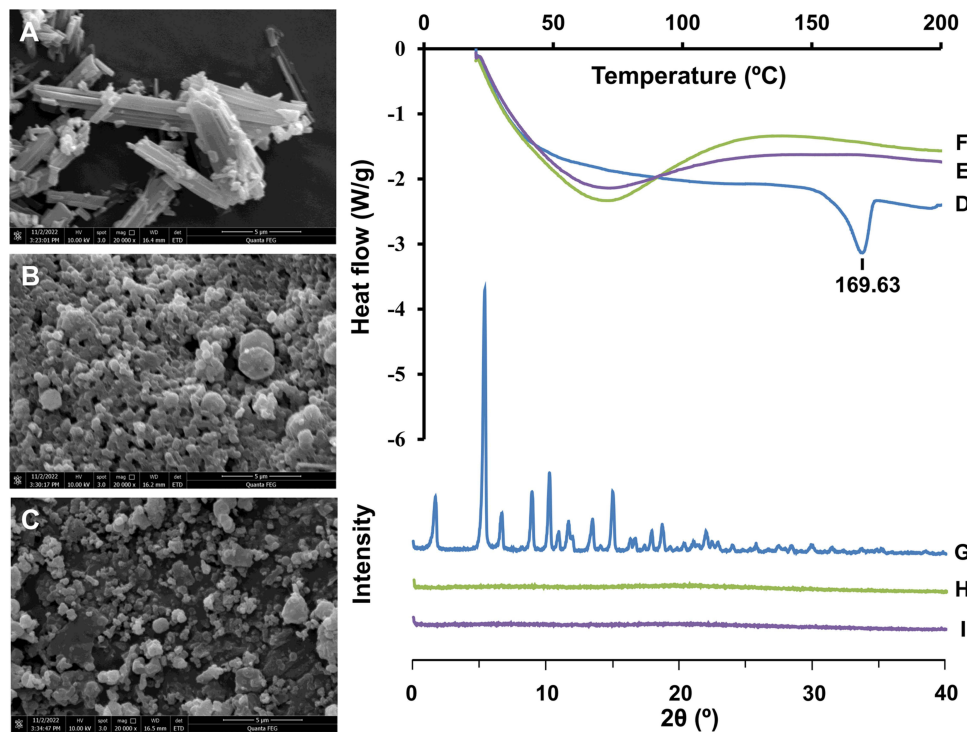


**Figure 2** Scanning electron microscopy observation (A–C; 20,000 ×), differential scanning calorimetry (D–F), and powder X-ray diffraction (G–I) images of docetaxel (A, D, G), the natural nanoparticles (Nnps) (B, F, H), and the self-assembled nanoparticles loaded with docetaxel (C, E, I).

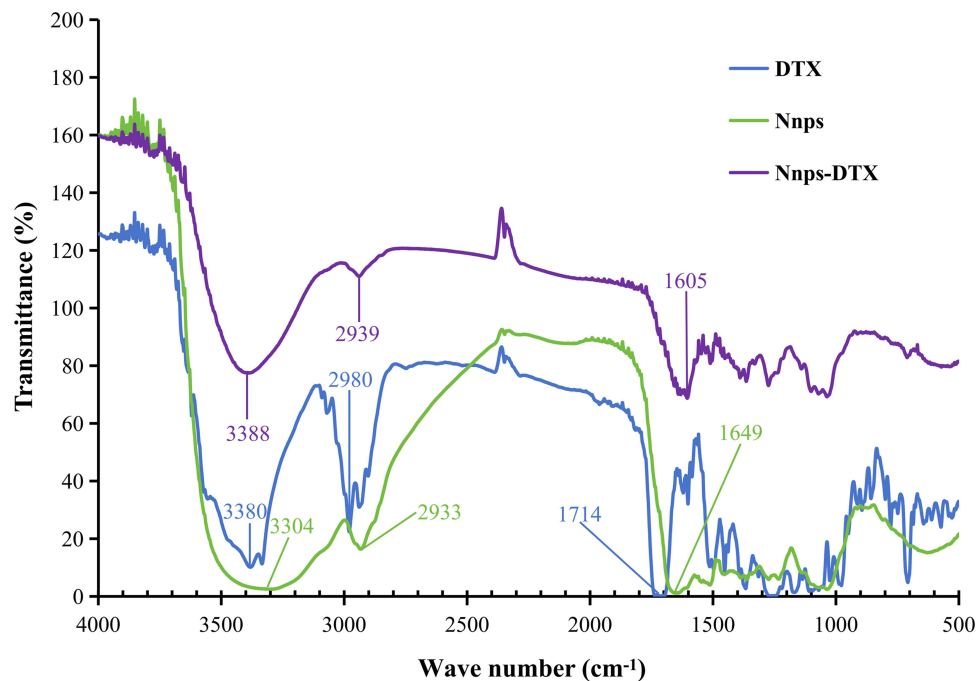


**Figure 3** Fourier transform infrared spectroscopy analysis of docetaxel (DTX), the natural nanoparticles (Nnps), and the self-assembled nanoparticles loaded with DTX (Nnps-DTX).

compared with Nnps (2933 cm<sup>-1</sup>) and DTX (2980 cm<sup>-1</sup>), and the peak shape and intensity were different from Nnps and DTX. These results imply potential hydrophobic interactions between DTX and Nnps within Nnps-DTX.<sup>32,33</sup> Moreover, the FTIR spectrum of Nnps-DTX revealed a significant shift in the peak at 1605 cm<sup>-1</sup> (indicative of C=O stretching)

compared to that of Nnps ( $1649\text{ cm}^{-1}$ ), along with a markedly different peak shape. These findings suggest the involvement of electrostatic interactions in the intermolecular interactions between DTX and Nnps within Nnps-DTX.<sup>32,33</sup>

### Solubility and dissolution of DTX

As shown in Figure 4A, the solubility of DTX in Nnps-DTX was significantly increased to approximately 23.3 times that of the control group ( $164.3\text{ }\mu\text{g/mL}$  vs  $7.0\text{ }\mu\text{g/mL}$ ,  $p < 0.01$ ).

Compared to the DTX group, the release of DTX in Nnps-DTX exhibited a significant increase, reaching 7.3% ( $p < 0.01$ ) within 2 hours in artificial gastric fluid (Figure 4B) and 62.5% ( $p < 0.01$ ) within 8 hours in artificial intestinal fluid, respectively (Figure 4C).

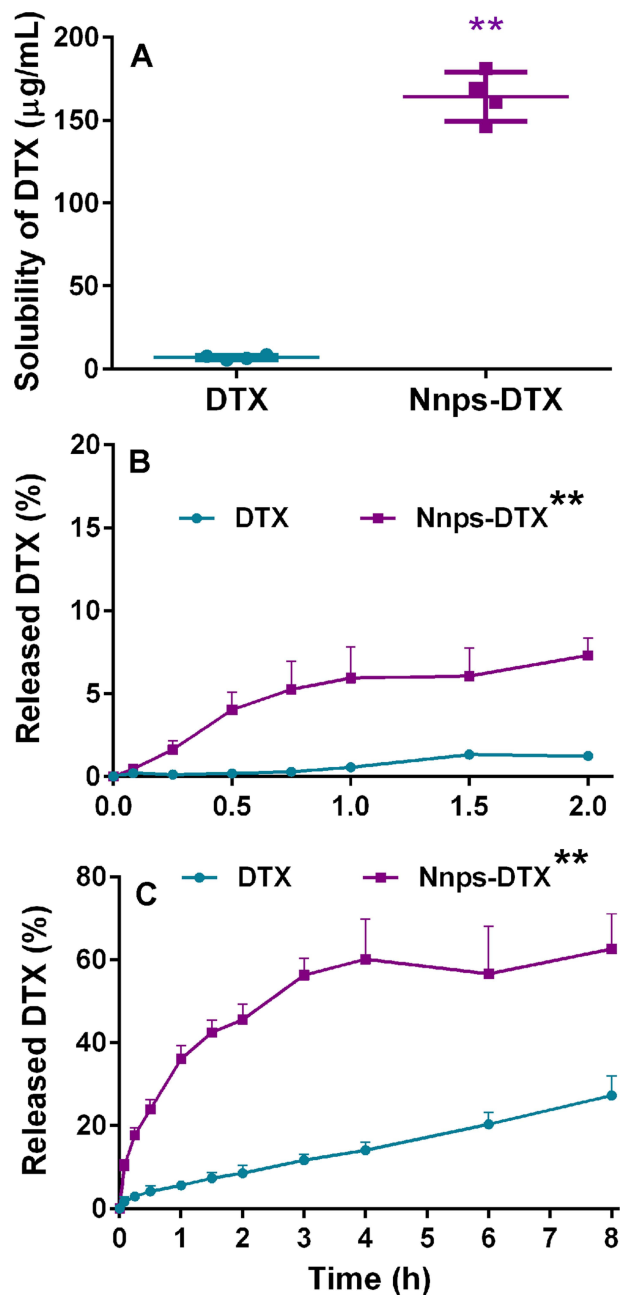


**Figure 4** Water solubility (A) and release of docetaxel (DTX) or DTX in the self-assembled nanoparticles (Nnps-DTX) containing the same amount of DTX in artificial gastric (B) or intestinal fluids (C) (mean  $\pm$  SD,  $n = 3$  for solubility;  $n = 4$  for release).  $**p < 0.01$  vs DTX.

## Metabolism of DTX in Liver Microsomes

As shown in Figure 5A, the percentage of metabolized DTX increased with incubation time, but DTX in Nnps-DTX showed better metabolic stability after incubation for 30 min and 90 min (both  $p < 0.01$ ).

## Uptake of DTX in Caco-2 Cells

As shown in Figure 5B, the uptake of DTX in Caco-2 cells was significantly increased in Nnps-DTX compared to the control group ( $p < 0.01$ ). In addition, indomethacin, a typical inhibitor of caveolae-mediated endocytosis, significantly reduced the uptake of DTX in Nnps-DTX by Caco-2 cells ( $p < 0.01$ ).

## Pharmacokinetics of DTX in Mice

The concentration-time curves of DTX in the portal vein, systemic circulation, liver and lung of mice in the oral DTX group and the oral Nnps-DTX group are shown in Figure 6, and the pharmacokinetic parameters are shown in Table 5. It is worth noting that due to the intermittent sampling in the mice, each pharmacokinetic parameter was calculated based on the average concentration of DTX in five mice at the corresponding time point, resulting in a sample size of 1 for each parameter.

In the mouse portal vein (Figure 6A),  $T_{max}$  was 1 h in the DTX group and 15 min in the Nnps-DTX group. The  $C_{max}$  and  $AUC_{0-12 h}$  of the Nnps-DTX group were approximately 8.8 and 1.8 times those of the DTX group, respectively.

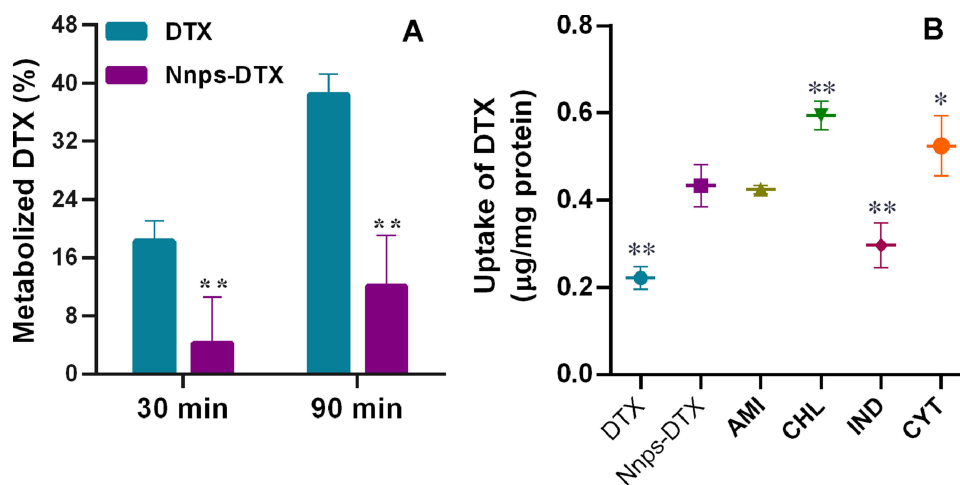
In the systemic circulation of the mice (Figure 6B), the  $T_{max}$  of both the DTX group and the Nnps-DTX group was 30 min. However, the  $C_{max}$  of the Nnps-DTX group was 23.4 times that of the DTX group, while the  $AUC_{0-12 h}$  was 7.8 times that of the DTX group.

In the mouse liver (Figure 6C), the  $T_{max}$  in the Nnps-DTX group was reduced from 0.5 h to 15 min compared to the DTX group. The  $C_{max}$  of the Nnps-DTX group was 44.6 times that of the DTX group, while the  $AUC_{0-12 h}$  was 8.5 times that of the DTX group.

In the lungs of the mice (Figure 6D),  $T_{max}$  was prolonged from 15 min to 30 min in the Nnps-DTX group compared to the DTX group. The  $C_{max}$  and  $AUC_{0-12h}$  of the Nnps-DTX group were 5.7 and 23.5 times those of the DTX group, respectively.

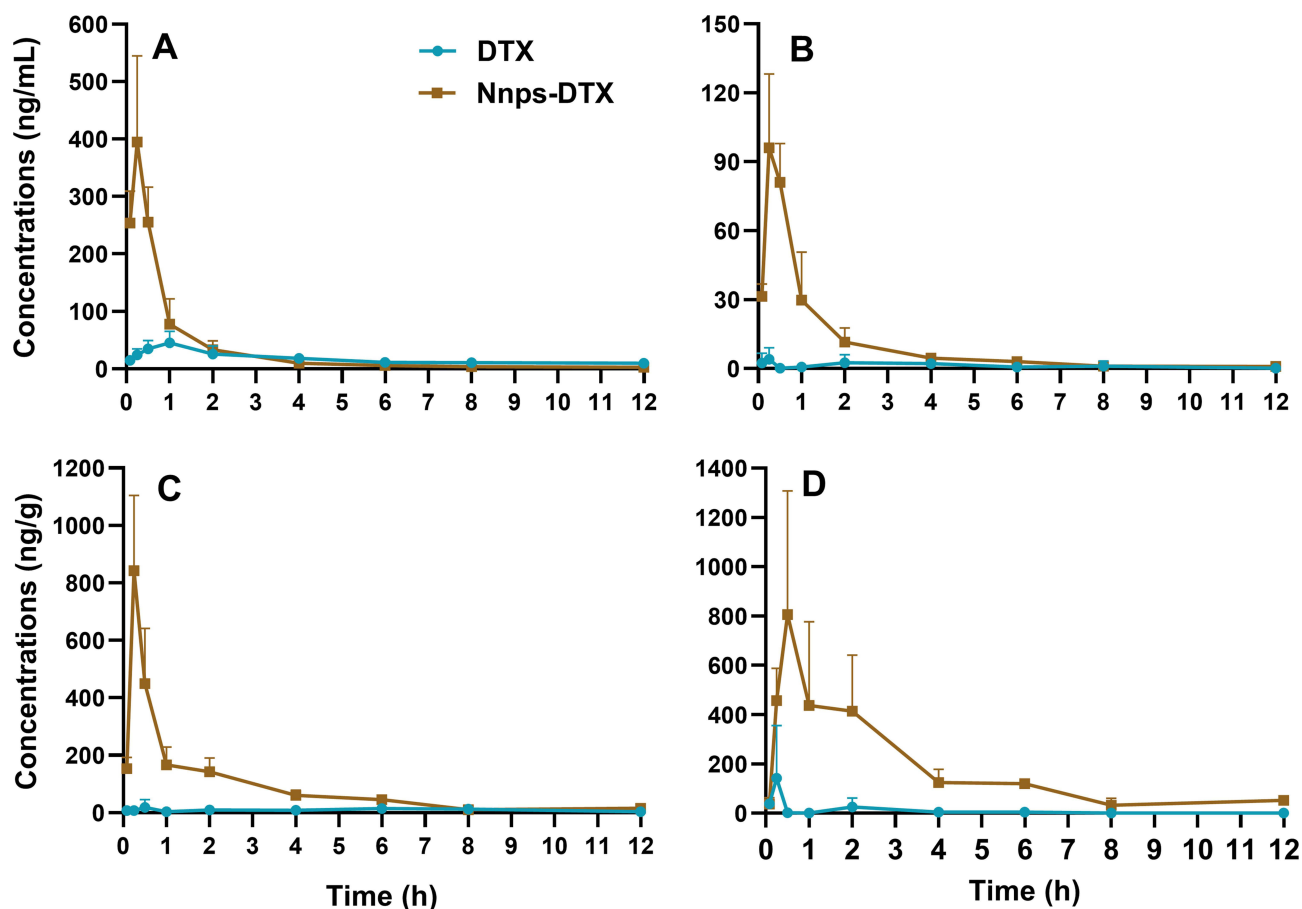
## In vitro Cytotoxicity of Nnps-DTX

Figure 7 illustrates the inhibitory effects of Nnps, DTX and Nnps-DTX on HepG2, MCF-7, and HCT116 cell viability. The results demonstrated that Nnps did not exert a significant impact on the viability of cancer cells, with  $IC_{50}$  values exceeding 3764 ng/mL (Figure 7A). Notably, the  $IC_{50}$  values for DTX and Nnps-DTX differed significantly ( $p < 0.01$ ) in



**Figure 5** In vitro metabolism (A) and uptake (B) of docetaxel (DTX) or DTX in self-assembled nanoparticles (Nnps-DTX) containing the same amount of DTX (mean  $\pm$  SD,  $n = 3$ ). A, Metabolism of DTX (10  $\mu$ M) in mouse liver microsomes. \*\*,  $p < 0.01$  vs DTX. B, Uptake of DTX (10  $\mu$ M) by Caco-2 cells and effects of endocytosis inhibitors. \*,  $p < 0.05$ ; \*\*,  $p < 0.01$  vs Nnps-DTX.

**Abbreviations:** AMI, amiloride (2.5 mM); CHL, chlorpromazine (10  $\mu$ g/mL); CYT, cytochalasin D (5  $\mu$ M); IND, indomethacin (100  $\mu$ g/mL).



**Figure 6** Concentration-time curves of docetaxel (DTX) in the portal vein (A), systemic circulation (B), liver (C), and lung (D) of the mice after oral administration of 20 mg/kg DTX or the self-assembled nanoparticles (Nnps-DTX) containing the same dose of DTX (mean  $\pm$  SD,  $n = 5$ ).

HepG2 cells (Figure 7B), indicating that Nnps-DTX exhibited stronger cytotoxicity against HepG2 cells compared to DTX. However, both DTX and Nnps-DTX displayed similar cytotoxicity in breast cancer MCF-7 (Figure 7C) and colon cancer HCT116 (Figure 7D), as evidenced by comparable  $IC_{50}$  values ( $p > 0.05$ ).

**Table 5** Pharmacokinetic Parameters of Docetaxel (Mean,  $n = 5$ )

Sites	Drugs	$T_{max}$ (h)	$C_{max}^a$	$T_{1/2}$ (h)	$AUC_{0-12\ h}^b$	MRT (h)
Portal Vein	DTX	1.00	45.0	34.1	202.1	4.4
	Nnps-DTX	0.25	394.6	6.3	366.2	1.5
Systemic Circulation	DTX	0.25	4.1	2.6	14.7	4.3
	Nnps-DTX	0.25	96.0	2.2	114.1	1.7
Liver	DTX	0.5	18.9	2.7	115.4	5.7
	Nnps-DTX	0.25	842.6	2.4	975.6	2.4
Lung	DTX	0.25	142.1	0.6	86.8	1.8
	Nnps-DTX	0.5	805.8	3.1	2037.2	3.0

**Notes:** <sup>a</sup> The unit for "portal vein" and "systemic circulation" is ng/mL, but ng/g for "liver" and "lungs"; <sup>b</sup> The unit for "portal vein" and "systemic circulation" is h ng/mL, but h ng/g for "liver" and "lung".

**Abbreviations:** AUC, the area under the concentration-time curve;  $C_{max}$ , peak concentration; DTX, docetaxel; MRT, mean retention time; Nnps-DTX, the DTX loaded nanoparticles;  $T_{1/2}$ , elimination half-life;  $T_{max}$ , time to reach peak concentration.

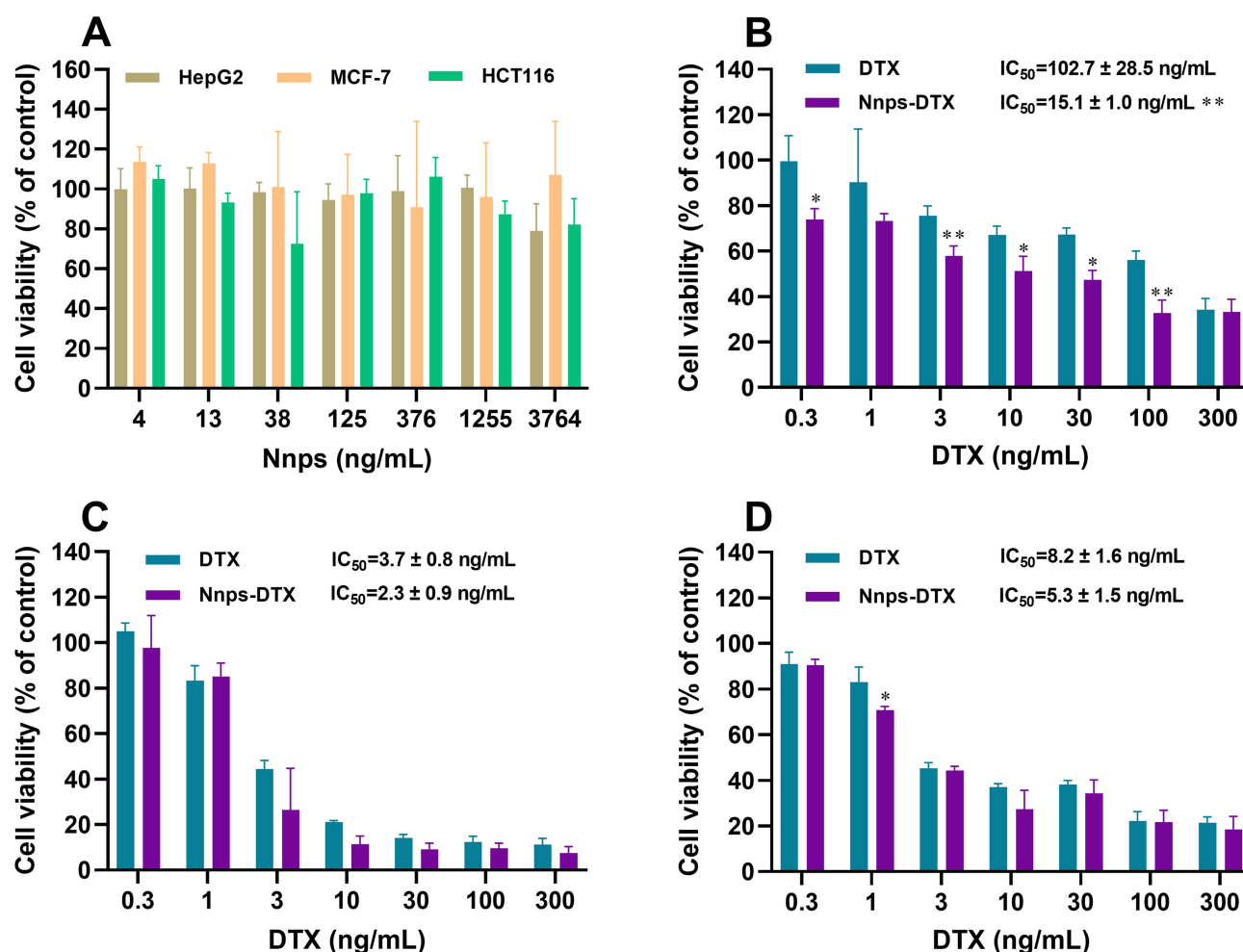


**Figure 7** Cytotoxicity of the natural nanoparticles (Nnps, **A**), docetaxel (DTX) and the self-assembled nanoparticles loaded with DTX (Nnps-DTX) against liver cancer HepG2 (**B**), breast cancer MCF-7 (**C**), and colon cancer HCT116 (**D**) cells (mean  $\pm$  SD,  $n=3$ ). \*,  $p < 0.05$ , \*\*,  $p < 0.01$  compared to the corresponding DTX group.

## Discussion

Under the influence of certain physical or chemical factors, protein molecules disintegrate and the structure is loosened so that a large number of hydrophobic groups, originally located inside the molecule, are exposed to the surface of the molecule.<sup>34</sup> When the confounding factors are removed, the dissociated subunits or components can reassemble to form an ordered architecture, such as nanoparticles.<sup>34</sup> Hydrophobic drugs can bind proteins through hydrophobic interactions, electrostatic interactions, and covalent interactions.<sup>35</sup> This means that under certain physical or chemical conditions, proteins can self-assemble with drugs to form drug-loaded nanoparticles. Nanoparticles formed by protein self-assembly can have good water solubility due to the distribution of hydrophilic groups on their surface, thereby increasing the apparent water solubility of the loaded drug.<sup>35</sup>

Methods commonly used to induce protein self-assembly include pH-induced dissociation and re-association, alcohol-induced dissociation (and/or denaturation) and reassembly, and heat-induced disassembly (or disassociation) and reassembly.<sup>34</sup> One of the major challenges in using protein self-assembly to form nanostructures is to determine the appropriate conditions for protein self-assembly into the desired structure.<sup>36</sup> Therefore, in this study, the preparation strategy of Nnps-DTX was first optimized. Random aggregation occurs when the environmental pH is close to the isoelectric point of the protein, and linear aggregation occurs when the pH is far from pI.<sup>37</sup> By changing the pH of the environment, proteins can be induced to self-assemble and encapsulate drugs, especially poorly water-soluble drugs.<sup>38</sup> This study showed that the pH-shifting strategy of incubating Nnps under alkaline conditions and then restoring neutrality produced Nnps-DTX with good properties. However, the size of the nanoparticles was relatively large. Furthermore, whereas DTX is highly stable in acidic

solutions and under heating, it degrades by about 25% after two hours of incubation in an alkaline solution (0.005 N NaOH, pH roughly 11.7).<sup>39</sup> As a result, pH-shifting strategy is inappropriate for Nnps-DTX preparation. Ethanol changes the structure or conformation of proteins mainly by reducing the polarity of the solvent.<sup>34</sup> In the present study, Nnps was induced by different concentrations of ethanol to form micron-sized particles with poor Zeta potential and PDI. On the contrary, Nnps was slowly denatured at a relatively mild temperature (65°C) and self-assembled into nanoparticles with ideal size, Zeta potential and PDI value after stirring together with DTX. Therefore, Nnps-DTX was prepared by heat-induced self-assembly in the subsequent experiments.

The preparation protocol of Nnps-DTX based on the heat-induction strategy was further optimized in this study. Protein self-assembly upon heating is highly dependent on environmental conditions (such as pH), heating conditions (such as temperature), protein (such as Nnps in this study) concentration and the presence of other compounds (such as DTX in this study).<sup>34</sup> In general, increasing the protein concentration within a certain range will reduce the intermolecular distance and increase the intermolecular interactions between the protein and the drug (in this case DTX) to form nanoparticles with smaller particle sizes.<sup>40</sup> However, if the protein concentration is too high (for example, 3 mg/mL in this study), protein aggregation occurs and the particle size increases. When the DTX/Nnps ratio was in a relatively low range, the particle size of the prepared Nnps-DTX decreased with increasing DTX/Nnps ratio, suggesting that DTX could drive the self-assembly of Nnps in a certain concentration range. According to the literature,<sup>34</sup> hydrophobic interactions may be formed between Nnps and DTX. However, when the DTX/Nnps ratio was too high, the particle size of the prepared Nnps-DTX increased, which may be due to the precipitation of DTX entrapped in the nanoparticles or adsorbed on the surface of the nanoparticles due to low solubility.<sup>40</sup> The results of the orthogonal experiment and the analysis of variance provided the optimal conditions for the preparation of Nnps-DTX, which were consistent with the results of the single factor experiments. Verification experiments showed that the preparation process was repeatable and reliable. In addition, the particle size, Zeta potential and PDI of the nanoparticles did not change significantly after lyophilisation, indicating that lyophilisation had little effect on Nnps-DTX, so no protective agent was added prior to lyophilisation in the subsequent preparation of the nanoparticles.

Nnps-DTX was less than 200 nm in size, which would help it escape phagocytosis by reticuloendothelial phagocytes (macrophages).<sup>41</sup> Nevertheless, based on the results of SEM and DLS analysis, the morphology of nanoparticles exhibited non-uniformity, and variations in size (ie, PDI) were observed, which reflect the inherent limitations of naturally formed macromolecular nanoparticles.<sup>35</sup> The Zeta potential of Nnps-DTX was lower than -20 mV, indicating that it does not tend to agglomerate. The *in vitro* stability results based on DLS analysis verified that Nnps-DTX was stable in water within 0–6 h. The result indicated that the nanoparticles would not significantly agglomerate or precipitate during administration of the water solution of the freeze-dried powder of the nanoparticles. Moreover, Nnps-DTX was stable in water and artificial gastric and intestinal fluids lacking digestive enzymes. However, upon incubation in the solutions containing the digestive enzymes, Nnps-DTX's size and PDI significantly increased. Since proteins comprise most of the nanoparticles, these results are easily understood. The absorption of Nnps-DTX would be hindered by its enlarged size. However, cells can uptake particles smaller than 500 nm via caveolae-mediated endocytosis.<sup>42</sup> On the other hand, the effects of digestive enzymes would help release DTX from the nanoparticles. As a result, there were both beneficial and unfavorable effects of digestive enzymes on DTX intestinal absorption.

Nnps-DTX had good encapsulation efficiency. However, proteins as drug carriers generally have the limitation of low drug loading due to the limited binding sites on the protein surface.<sup>34</sup> The DTX content of Nnps-DTX in this study was approximately 7.97%, which means that the nanoparticle dose equivalent to a 20 mg/kg dose of DTX would be approximately 250 mg/kg, which is acceptable for oral administration.

Under SEM, no intrinsic columnar crystal structure of DTX was observed in Nnps-DTX. The results of DSC and PXRD also showed that DTX did not exist in crystalline form in the nanoparticles. These results suggest that DTX may be embedded in the nanoparticles or exist in an amorphous form. FTIR is widely used to evaluate intermolecular interactions.<sup>31–33</sup> The results of FTIR analysis revealed that hydrogen bonds, hydrophobic interactions, and electrostatic interactions were involved in the formation of Nnps-DTX. Furthermore, in the FTIR spectra of Nnps-DTX, the characteristic absorption peaks of DTX shifted and the intensity decreased or even disappeared, suggesting that DTX was encapsulated or existed in an amorphous form in Nnps-DTX. The results are in agreement with those of SEM, DSC, and PXRD. In addition, the FTIR spectra of Nnps-DTX showed that the absorption peak of Nnps at 1649 cm<sup>-1</sup> had



shifted, indicating that the secondary structure of Nnps had changed after DTX loading.<sup>30</sup> However, it is still unknown what the exact secondary structure of Nnps is and how much it changes quantitatively following DTX loading.

The usual dose of DTX in mice is 20 mg/kg.<sup>4</sup> Therefore, if DTX is administered at 0.2 mL/10 g body weight, it should be administered at a concentration of 1 mg/mL. However, the present study showed that the solubility of DTX was as low as 7.0 µg/mL, which means that more than 99% of DTX was not dissolved when administered *in vivo*. Thus, low solubility is one of the main reasons limiting the oral bioavailability of DTX. The experimental results show that the solubility of DTX was significantly improved in Nnps-DTX, which is about 23.3 times higher than that of DTX. In addition, the drug release experiment based on the dialysis method showed that the dissolution of DTX in Nnps-DTX was significantly improved in both artificial gastric and intestinal fluids. An acceptable explanation is that the drug in its amorphous form usually has better solubility and dissolution than the crystalline form.<sup>43</sup> The release of DTX in Nnps-DTX was limited in artificial gastric fluids and predominantly in artificial intestinal fluids, demonstrating intestinal-targeted release properties. The slight structural changes of Nnps-DTX, namely the increase of size and PDI found in the *in vitro* stability experiment, explained its good release in artificial intestinal fluid. DTX in Nnps-DTX was released slowly after 4 h of sustained release in artificial intestinal fluid. The initial rapid release of DTX in Nnps-DTX may be due to the rapid release of DTX adsorbed on the surface of the nanoparticles. With increasing time, the dissolution of DTX decreased slightly, which may be due to the accumulation of some free DTX in the dissolution medium.

Pharmacokinetic studies showed that the intestinal absorption of DTX was significantly increased in Nnps-DTX compared to DTX after oral administration, resulting in increased AUC<sub>0-12 h</sub> and C<sub>max</sub> of DTX in the portal vein and systemic circulation. Nanoparticles are taken up by intestinal cells mainly by macropinocytosis, phagocytosis, clathrin-mediated endocytosis and caveolae-mediated endocytosis,<sup>44</sup> which could be selectively inhibited by the compounds amiloride,<sup>27</sup> cytochalasin D,<sup>27</sup> chlorpromazine,<sup>26</sup> and indomethacin.<sup>26</sup> Caco-2 cells are widely used as an intestinal epithelial cell model for *in vitro* uptake and absorption studies. The results showed that the uptake of DTX in Nnps-DTX was significantly higher than that of DTX in Caco-2 cells. Meanwhile, indomethacin inhibited the cellular uptake of DTX in Nnps-DTX, suggesting that Nnps-DTX may be taken up by caveolae-mediated endocytosis.<sup>26,45</sup> Caveolae can mediate cellular uptake of nanoparticles ranging in size from less than 100 nm<sup>46</sup> to more than 200 nm<sup>47</sup> or even 500 nm.<sup>42</sup> One of the advantages of caveolae-mediated endocytosis is that nanoparticles can bypass lysosomal degradation and be transported across cells as intact nanoparticles.<sup>44</sup> Chlorpromazine and cytochalasin D promoted the uptake of DTX in Nnps-DTX in this study, which might be related to their inhibitory effect on the transporter p-glycoprotein (P-gp).<sup>48,49</sup> It was reported that P-gp mediates the efflux of DTX.<sup>50</sup> However, the process and mechanism of Nnps-DTX uptake *in vivo* would be much more complex and needs to be further elucidated. In addition, DTX may be eliminated by metabolism during intestinal absorption and tissue distribution, particularly liver distribution.<sup>1</sup> The *in vitro* metabolism results showed that Nnps-DTX had better metabolic stability than DTX. The improved metabolic stability contributed to the increased absorption and *in vivo* exposure of DTX in Nnps-DTX.

Clinically, DTX injections are used to treat non-small cell lung cancer.<sup>3</sup> The high exposure levels of DTX in the lung suggest that Nnps-DTX has the potential to be used orally for the treatment of lung tumors. Similarly, the high exposure levels in the liver suggest a potential application of oral Nnps-DTX in liver tumors. The significant increase in DTX distribution in the liver and lung may be due to the increased concentration and prolonged exposure time of DTX in the circulation. In addition, the high vascular permeability of the lung and liver facilitates the entry of nanoparticles. These results suggest that Nnps-DTX in the form of nanoparticles can be distributed in tissues with good vascular permeability after absorption. However, one of the limitations of this study is that it did not ascertain the *in vivo* absorption and tissue distribution of Nnps-DTX as nanoparticles. The *in vivo* imaging results revealed the presence of DiR fluorescence in the liver following oral administration of DiR-labeled Nnps (data not shown). However, this finding does not rule out the possibility that free DiR molecules rather than DiR-labeled nanoparticles entered the liver. Such studies are still technically challenging. Cell-based assays showed that Nnps-DTX had a better anti-tumor effect than DTX on HepG2 cells. The findings suggest that oral administration of Nnps-DTX may augment the efficacy of DTX by increasing its exposure or facilitating direct distribution into the liver. However, further *in vivo* research is needed to fully explore the potential antitumor effects of orally administered Nnps-DTX.

## Conclusions

In this study, a novel type of self-assembled nanoparticles loaded with DTX was constructed. DTX was present in Nnps-DTX in an amorphous form, which significantly improved its solubility and release. In addition, DTX in Nnps-DTX had good cellular uptake and metabolic stability. Due to these mechanisms, the intestinal absorption, pharmacokinetic properties and tissue distribution of DTX in Nnps-DTX were significantly improved. In addition, Nnps-DTX had strong inhibitory effects on cell viability of MCF-7, HCT116 and especially HepG2 cells. In brief, the innovative self-assembled protein nanoparticles, significantly improved the solubility, release, cellular uptake, metabolic stability, and pharmacokinetics of oral DTX, and exhibited substantial cytotoxicity against tumor cell lines. We believe that this study provides a viable delivery system for oral DTX administration, which is worthy of further development.

## Abbreviations

AUC, the area under the concentration-time curve; BCA, diquinolinic acid; BSA, bovine serum albumin; Caco-2, human colonic adenocarcinoma cells;  $C_{max}$ , peak concentration; DiR, 1, 1-dioctadecyl-3, 3, 3- tetramethylindotricarbocyanine iodide; DL, drug loading; DMEM, Dulbecco's modified Eagle's medium; DMSO, dimethyl sulfoxide; DSC, differential scanning calorimetry; DTX, docetaxel; EE, encapsulation efficiency; HBSS, Hank's balanced salt solution; HSA, human serum albumin; LC-MS/MS, liquid chromatography-tandem mass spectrometry; MRT, mean retention time; NADPH, reduced nicotinamide adenine dinucleotide phosphate; Nnps-DTX, the self-assembled nanoparticles loaded with DTX; PDI, polydispersity index; PXRD, powder X-ray diffraction; SEM, scanning electron microscopy;  $T_{1/2}$ , elimination half-life; TCMs, traditional Chinese medicines;  $T_{max}$ , time to reach peak concentration; UPLC, ultra-performance liquid chromatography.

## Data Sharing Statement

The datasets and materials used and/or analyzed during the current study are available from the corresponding author, Bing-Liang Ma, on request.

## Ethics Approval and Informed Consent

All animal experiments were approved by the Institutional Animal Care and Use Committee of Shanghai University of Traditional Chinese Medicine (SHUTCM), with the approved number of PZSHUTCM211018015. The animal experiments were performed according to the guidelines of the committee in the experimental animal center of SHUTCM.

## Consent for Publication

Not applicable.

## Declaration of Generative AI and AI-Assisted Technologies in the Writing Process

During the preparation of this work the authors used ChatGPT 3.5 in order to check grammar and spelling. After using this tool, the authors reviewed and edited the content as needed and take full responsibility for the content of the publication.

## Funding

This work was financially supported by the National Natural Science Foundation of China (82274356).

## Disclosure

The authors declare that they have no competing interests in this work.

## References

1. Imran M, Saleem S, Chaudhuri A, Ali J, Baboota S. Docetaxel: an update on its molecular mechanisms, therapeutic trajectory and nanotechnology in the treatment of breast, lung and prostate cancer. *J Drug Deliv Sci Tec.* 2020;60:101959. doi:10.1016/j.jddst.2020.101959
2. Swain SM, Baselga J, Kim SB, et al. Pertuzumab, trastuzumab, and docetaxel in HER2-positive metastatic breast cancer. *N Engl J Med.* 2014;372(8):724–734. doi:10.1056/NEJMoa1413513
3. Borghaei H, Paz-Ares L, Horn L, et al. Nivolumab versus docetaxel in advanced nonsquamous non-small-cell lung cancer. *N Engl J Med.* 2015;373(17):1627–1639. doi:10.1056/NEJMoa1507643
4. Jha SK, Chung JY, Pangeni R, et al. Enhanced antitumor efficacy of bile acid-lipid complex-anchored docetaxel nanoemulsion via oral metronomic scheduling. *J Control Release.* 2020;328:368–394. doi:10.1016/j.jconrel.2020.08.067
5. Baker J, Ajani J, Scotte F, et al. Docetaxel-related side effects and their management. *Eur J Oncol Nurs.* 2009;13(1):49–59. doi:10.1016/j.ejon.2008.10.003
6. Sohail MF, Rehman M, Sarwar HS, et al. Advancements in the oral delivery of docetaxel: challenges, current state-of-the-art and future trends. Review. *Int J Nanomed.* 2018;13:3145–3161. doi:10.2147/IJN.S164518
7. McClements DJ. Advances in nanoparticle and microparticle delivery systems for increasing the dispersibility, stability, and bioactivity of phytochemicals. *Biotechnol Adv.* 2020;38:107287. doi:10.1016/j.biotechadv.2018.08.004
8. Kianfar E. Protein nanoparticles in drug delivery: animal protein, plant proteins and protein cages, albumin nanoparticles. *J Nanobiotechnol.* 2021;19(1):159. doi:10.1186/s12951-021-00896-3
9. Elzoghby AO, Samy WM, Elgindy NA. Albumin-based nanoparticles as potential controlled release drug delivery systems. *J Control Release.* 2012;157(2):168–182. doi:10.1016/j.jconrel.2011.07.031
10. Yardley DA. nab-Paclitaxel mechanisms of action and delivery. *J Control Release.* 2013;170(3):365–372. doi:10.1016/j.jconrel.2013.05.041
11. Tang XL, Wang GJ, Shi RJ, et al. Enhanced tolerance and antitumor efficacy by docetaxel-loaded albumin nanoparticles. *Drug Deliv.* 2016;23(8):2686–2696. doi:10.3109/10717544.2015.1049720
12. Zhang Y, Zhang H, Wang J, et al. Reduction-responsive docetaxel prodrug encapsulated within human serum albumin nanoparticles for cancer therapy. *Mol Pharm.* 2023;20(5):2513–2526. doi:10.1021/acs.molpharmaceut.2c01107
13. Desale JP, Swami R, Kushwah V, Katiyar SS, Jain S. Chemosensitizer and docetaxel-loaded albumin nanoparticle: overcoming drug resistance and improving therapeutic efficacy. *Nanomedicine-UK.* 2018;13(21):2759–2776. doi:10.2217/nnm-2018-0206
14. Yu Z, Li X, Duan J, Yang X-D. Targeted treatment of colon cancer with aptamer-guided albumin nanoparticles loaded with docetaxel. *Int J Nanomed.* 2020;15:6737–6748. doi:10.2147/IJN.S267177
15. Lee HS, Kang N-W, Kim H, et al. Chondroitin sulfate-hybridized zein nanoparticles for tumor-targeted delivery of docetaxel. *Carbohydr Polym.* 2021;253:117187. doi:10.1016/j.carbpol.2020.117187
16. Chiu HI, Lim V. Wheat germ agglutinin-conjugated disulfide cross-linked alginate nanoparticles as a docetaxel carrier for colon cancer therapy. *Int J Nanomed.* 2021;16:2995–3020. doi:10.2147/IJN.S302238
17. Zhang L, Xiao QQ, Wang YR, Zhang CS, He W, Yin LF. Denatured protein-coated docetaxel nanoparticles: alterable drug state and cytosolic delivery. *Int J Pharmaceut.* 2017;523(1):1–14. doi:10.1016/j.ijpharm.2017.03.026
18. Ma B-L, Ma Y-M. Pharmacokinetic properties, potential herb-drug interactions and acute toxicity of oral *Rhizoma coptidis* alkaloids. *Expert Opin Drug Metab Toxicol.* 2013;9(1):51–61. doi:10.1517/17425255.2012.722995
19. Zhao J, Zhao Q, Lu JZ, et al. Natural nano-drug delivery system in *coptidis rhizoma* extract with modified berberine hydrochloride pharmacokinetics. *Int J Nanomed.* 2021;16:6297–6311. doi:10.2147/IJN.S323685
20. B-L M, Yin C, Zhang B-K, et al. Naturally occurring proteinaceous nanoparticles in *Coptidis Rhizoma* extract act as concentration-dependent carriers that facilitate berberine absorption. *Sci Rep.* 2016;6(1):20110. doi:10.1038/srep20110
21. Ma BL, Ma YM, Shi R, et al. Identification of the toxic constituents in *Rhizoma Coptidis*. *J Ethnopharmacol.* 2010;128(2):357–364. doi:10.1016/j.jep.2010.01.047
22. Yang Y, Vong CT, Zeng S, et al. Tracking evidences of *Coptis chinensis* for the treatment of inflammatory bowel disease from pharmacological, pharmacokinetic to clinical studies. *J Ethnopharmacol.* 2021;268:113573. doi:10.1016/j.jep.2020.113573
23. Park C, Meghani NM, Shin Y, et al. Investigation of crystallization and salt formation of poorly water-soluble telmisartan for enhanced solubility. *Pharmaceutics.* 2019;11(3):102. doi:10.3390/pharmaceutics11030102
24. National Pharmacopoeia Committee. Dissolution and release assay. *Pharmacopoeia of the People's Republic of China.* 2020;4:132–136.
25. Berardi A, Evans DJ, Baldelli Bombelli F, Lomonosoff GP. Stability of plant virus-based nanocarriers in gastrointestinal fluids. *Nanoscale.* 2018;10(4):1667–1679. doi:10.1039/c7nr07182e
26. Mahmood A, Prufert F, Efiana NA, et al. Cell-penetrating self-nanoemulsifying drug delivery systems (SNEDDS) for oral gene delivery. *Expert Opin Drug Deliv.* 2016;13(11):1503–1512. doi:10.1080/17425247.2016.1213236
27. Wadia JS, Stan RV, Dowdy SF. Transducible TAT-HA fusogenic peptide enhances escape of TAT-fusion proteins after lipid raft macropinocytosis. *Nat Med.* 2004;10(3):310–315. doi:10.1038/nm996
28. Fang GH, Tang B, Liu ZT, et al. Novel hydrophobin-coated docetaxel nanoparticles for intravenous delivery: in vitro characteristics and in vivo performance. *Eur J Pharm Sci.* 2014;60:1–9. doi:10.1016/j.ejps.2014.04.016
29. Hammadi NI, Abba Y, Hezme MNM, et al. Formulation of a sustained release docetaxel loaded cockle shell-derived calcium carbonate nanoparticles against breast cancer. *Pharm Res.* 2017;34(6):1193–1203. doi:10.1007/s11095-017-2135-1
30. Ahmed-Ouameur A, Diamantoglou S, Sedaghat-Herati MR, Nafisi S, Carpentier R, Tajmir-Riahi HA. The effects of drug complexation on the stability and conformation of human serum albumin: protein unfolding. *Cell Biochem Biophys.* 2006;45(2):203–213. doi:10.1385/cbb.45:2:203
31. Tang B, Fang G, Gao Y, et al. Liposomes loading paclitaxel for brain-targeting delivery by intravenous administration: in vitro characterization and in vivo evaluation. *Int J Pharm.* 2014;475(1–2):416–427. doi:10.1016/j.ijpharm.2014.09.011
32. Yu N, Wang J, Jiang C, et al. Development of composite nanoparticles from gum Arabic and carboxymethylcellulose-modified *Stauntonia brachyanthera* seed albumin for lutein delivery. *Food Chem.* 2022;372:131269. doi:10.1016/j.foodchem.2021.131269

33. Shinde P, Agraval H, Srivastav AK, Yadav UCS, Kumar U. Physico-chemical characterization of carvacrol loaded zein nanoparticles for enhanced anticancer activity and investigation of molecular interactions between them by molecular docking. *Int J Pharm.* 2020;588:119795. doi:10.1016/j.ijpharm.2020.119795
34. Tang CH. Strategies to utilize naturally occurring protein architectures as nanovehicles for hydrophobic nutraceuticals. *Food Hydrocolloid.* 2021;112:106344. doi:10.1016/j.foodhyd.2020.106344
35. Lin Q, Ge S, McClements DJ, et al. Advances in preparation, interaction and stimulus responsiveness of protein-based nanodelivery systems. *Crit Rev Food Sci.* 2021;1997908. doi:10.1080/10408398.2021.1997908.
36. Tang C-H. Assembly of food proteins for nano- encapsulation and delivery of nutraceuticals (a mini-review). *Food Hydrocolloid.* 2021;117:106710. doi:10.1016/j.foodhyd.2021.106710
37. Teng XR, Shchukin DG, Mohwald H. Encapsulation of water-immiscible solvents in polyglutamate/polyelectrolyte nanocontainers. *Adv. Funct. Mater.* 2007;17(8):1273–1278. doi:10.1002/adfm.200601229
38. Zhang J, Hassane Hamadou A, Chen C, Xu B. Encapsulation of phenolic compounds within food-grade carriers and delivery systems by pH-driven method: a systematic review. *Crit Rev Food Sci.* 2021;1998761. doi:10.1080/10408398.2021.1998761
39. Rao BM, Chakraborty A, Srinivasu MK, et al. A stability-indicating HPLC assay method for docetaxel. *J Pharm Biomed Anal.* 2006;41(2):676–681. doi:10.1016/j.jpba.2006.01.011
40. Asghar S, Salmani JMM, Hassan W, et al. A facile approach for crosslinker free nano self assembly of protein for anti-tumor drug delivery: factors' optimization, characterization and in vitro evaluation. *Eur J Pharm Sci.* 2014;63:53–62. doi:10.1016/j.ejps.2014.06.022
41. Choi JS, Cao J, Naeem M, et al. Size-controlled biodegradable nanoparticles: preparation and size-dependent cellular uptake and tumor cell growth inhibition. *Colloids Surf B Biointerfaces.* 2014;122:545–551. doi:10.1016/j.colsurfb.2014.07.030
42. Rejman J, Oberle V, Zuhorn IS, Hoekstra D. Size-dependent internalization of particles via the pathways of clathrin- and caveolae-mediated endocytosis. *Biochem J.* 2004;377(Pt 1):159–169. doi:10.1042/BJ20031253
43. Williams HD, Trevaskis NL, Charman SA, et al. Strategies to address low drug solubility in discovery and development. *Pharmacol Rev.* 2013;65(1):315–499. doi:10.1124/pr.112.005660
44. Sahay G, Alakhova DY, Kabanov AV. Endocytosis of nanomedicines. *J Control Release.* 2010;145(3):182–195. doi:10.1016/j.jconrel.2010.01.036
45. Canton I, Battaglia G. Endocytosis at the nanoscale. *Chem. Soc. Rev.* 2012;41(7):2718–2739. doi:10.1039/c2cs15309b
46. Iversen TG, Skotland T, Sandvig K. Endocytosis and intracellular transport of nanoparticles: present knowledge and need for future studies. *Nano Today.* 2011;6(2):176–185. doi:10.1016/j.nantod.2011.02.003
47. Rejman J, Conese M, Hoekstra D. Gene transfer by means of lipo- and polyplexes: role of clathrin and caveolae-mediated endocytosis. *J Liposome Res.* 2006;16(3):237–247. doi:10.1080/08982100600848819
48. Wang JS, Zhu HJ, Markowitz JS, Donovan JL, DeVane CL. Evaluation of antipsychotic drugs as inhibitors of multidrug resistance transporter P-glycoprotein. *Psychopharmacology (Berl).* 2006;187(4):415–423. doi:10.1007/s00213-006-0437-9
49. Trendowski M, Christen TD, Acquafondata C, Fondy TP. Effects of cytochalasin congeners, microtubule-directed agents, and doxorubicin alone or in combination against human ovarian carcinoma cell lines in vitro. *Bmc Cancer.* 2015;15(1):632. doi:10.1186/s12885-015-1619-9
50. Han SY, Kim ES, You BH, et al. Effect of treatment period with LC478, a disubstituted adamantyl derivative, on P-glycoprotein inhibition: its application to increase docetaxel absorption in rats. Article. *Xenobiotica.* 2020;50(7):863–874. doi:10.1080/00498254.2019.1700318

International Journal of Nanomedicine

Dovepress

## Publish your work in this journal

The International Journal of Nanomedicine is an international, peer-reviewed journal focusing on the application of nanotechnology in diagnostics, therapeutics, and drug delivery systems throughout the biomedical field. This journal is indexed on PubMed Central, MedLine, CAS, SciSearch®, Current Contents®/Clinical Medicine, Journal Citation Reports/Science Edition, EMBase, Scopus and the Elsevier Bibliographic databases. The manuscript management system is completely online and includes a very quick and fair peer-review system, which is all easy to use. Visit <http://www.dovepress.com/testimonials.php> to read real quotes from published authors.

Submit your manuscript here: <https://www.dovepress.com/international-journal-of-nanomedicine-journal>